

New 5,6-dihydro pyrimidin-2(1*H*)-thione compound containing imine moiety: synthesis, characterization, and nonlinear optical study

Jenan Al Ameri¹, H. A. Sultan², Mariam Abdul-Bary³, Qusay M. A. Hassan^{2,*}, Batool Haddad², and C. A. Emshary¹

Received: 17 September 2024 Accepted: 23 November 2024

© The Author(s), under exclusive licence to Springer Science+Business Media, LLC, part of Springer Nature, 2024

ABSTRACT

A novel chemical, 5,6-dihydro pyrimidin-2(1H)-thione (compound A), is synthesized and characterized using several analytical techniques including FTIR, 1H NMR, $^{13}CNMR$, and mass spectroscopies. The compound's structure has been determined. The nonlinear optical (NLO) properties of the compound are analyzed by subjecting it to visible continuous wave (cw), low power laser beams and observing the effects through the Z-scan and diffraction patterns. The initial approach yielded a nonlinear refractive index (NLRI) of 0.21×10^{-7} cm²/W, while the following method yielded an NLRI of 3.925×10^{-7} cm²/W. Each optical switching utilizes two laser beams: one beam controlled at a wavelength of 532 nm and another beam controlling at a wavelength of 473 nm.

1 Introduction

During the last four decades, enormous interest has been exerted to study nonlinear, naturally available materials [1–5], and other material properties have been modified by different techniques viz., irradiation with γ -rays [6–10] and new synthesized materials [11–20]. The occurrence of various nonlinear optical (NLO) phenomena is the results of the nonlinear refractive index (NLRI) being dependent on light intensity. By capitalizing on these events, scientists have developed several applications such as optical delay, optical limiting, all-optical modulation, and optical switching [21–24]. Materials with high third-order

nonlinear susceptibility, $\chi^{(3)}$, and fast response have attracted significant attention due to their potential applications stated earlier. One of the ways used to estimate the NLRI is the single beam Z-scan methodology, which was established by Sheikh-Bahae et al. [25, 26]. This method is simple and effective that is paired with diffraction patterns (DPs) [27, 28]. The first technique leads to measure the NLRI and assign its sign, while the second one used to measure the NLRI and the change in the medium refractive index (RI) based on the number of DPs at the maximum power input.

Due to the potential applications of α , β -unsaturated ketone derivatives, they have been attracted considerable interests as to their synthesize [29]. Practically,

Address correspondence to E-mail: qusayali64@yahoo.co.in

https://doi.org/10.1007/s10854-024-13975-6 Published online: 09 December 2024



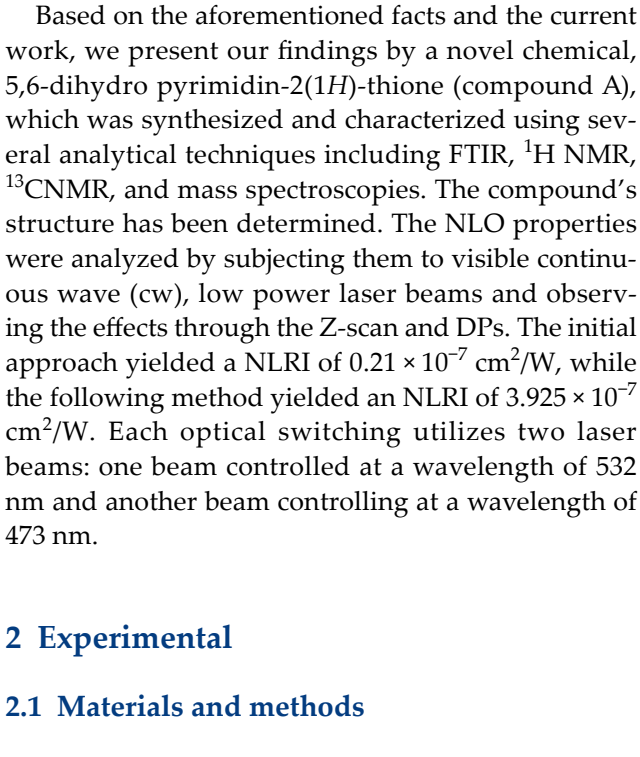
¹ Department of Chemistry, College of Science, University of Basrah, Basrah 61001, Iraq

² Department of Physics, College of Education for Pure Sciences, University of Basrah, Basrah 61001, Iraq

³ Department of Food Science, College of Agriculture, University of Basrah, Basrah 61001, Iraq

 α , β -unsaturated ketone has many applications due to the presence of an unsaturated α , β - and a functional group [30]. Furthermore, it is used in the synthesis of many drug treatments such as cancer drugs as well as antibiotics, insecticides, dyes, agriculture, and in many other fields [31]. The German scientist H. Schiff was the first to discover Schiff base in 1864. Schiff bases containing the azomethine group were prepared for the first time by condensing compounds containing the carbonyl group [32]. Their biological activity was shown to be attributed to a reactive unsaturated group found in α,β -unsaturated ketone. Recently, α,β unsaturated ketone has demonstrated potent cleaning properties, as reported by multiple sources [33]. In addition to its antioxidant effects, it is considered to be the basis for the creation of many heterocyclic compounds [34]. It has been used to prepare a variety of biologically and commercially useful compounds, such as 4-thiazolidinene, formazan, benzoxazine, cyclo-loading, ring-closure, and substitution procedures [35].

Heterocyclic oligomers and polymers are widely favored for their chemical, environmental, and electrical durability, making them a preferred option for incorporation into solar cells [36]. Pyrimidine compounds are categorized by occupying an outstanding class among other organic compounds. Pyrimidine compounds have a distinctive role to play in the field of synthesis of organic chemistry and natural products. They have been used to synthesize drugs for the treatment of diabetes, cancer, and other diseases. [37] Furthermore, pyrimidine compounds have also been used in the synthesis of agrochemicals and polymers. As they can be readily synthesized and display a unique reactivity, they are widely used in drug discovery and development [38]. Pyrimidine compounds have been explored for their potential to control cancer, boost immune system performance, and act as free radical scavengers [39]. The most probable mechanism mediating the preventive benefits against cancer formation is that they are able to minimize oxidative stress [40]. Oxidative stress is an imbalance between the generation of free radicals and reactive metabolites [41]. Antioxidants are also known as reactive oxygen species (ROS), and they have protective mechanisms that remove harmful oxidants. Important biomolecules and cells are subject to be damaged as a result of this imbalance, which has the potential to seriously affect the entire organism [42].



In accordance with literature procedures, the synthesized compound was prepared. One mole of aniline was used to react one mole of benzil to prepare imine compound. The resulted compound was used to react with acetone to prepare imine compound containing α , β -unsaturated ketone. In ethanol and glacial acetic acid as a catalyst, 5,6-dihydro pyrimidin-2(1*H*)-thione (compound A) was synthesized from α , β -unsaturated ketone and urea. A Shimadzu spectrometer was used to record FT-IR spectrum. A Bruker spectrometer was used to record NMR spectrum, 400 MHz, (¹H and ¹³ C) NMR. DMSO and Me₄Si were used as internal references for NMR measurements of ¹ H and ¹³ C. Shimadzu QP GC-MS was used to record mass spectrum. An electrothermal IA was used to quantify the compound A melting points.

2.2 The general procedure to synthesize 1,2-diphenyl-2-(phenylimino) ethan-1-one

(0.028) moles of benzil dissolved in 30 ml of absolute ethanol was added into a 100-ml one-neck round-bottomed flask and then a solution of aniline (0.028 mol) was added [43, 44]. After raising the temperature of the reaction mixture to 78 °C, it was allowed to undergo reflux for a duration of six hours in the absence of light. The development of the reactions was monitored using thin-layer chromatography (TLC). Once the



reaction mixture cooled, the precipitate was filtered and recrystallized using 100% ethanol. The physical properties of the product are as follows: light yellow; Yield: 87%; M.p.: 180–181 °C; FT-IR stretching vibration v (cm⁻¹): 1678 (C=O), 1590 (C=N), 1488 (C=C), 3095 (C–H aromatic); ¹H NMR [400 MHz, DMSO, δ (ppm)]: 6.43–7.24 (15 H, aromatic).

2.3 The general procedure to synthesize 4,5-diphenyl-5-(phenylimino) pent-3-en-2-one

In a 100-ml one-necked round-bottomed flask, (0.028 mol) of benzil containing imine group was mixed with 30 ml of acetone [45, 46]. A solution was prepared by combining 5 g of sodium hydroxide with 50 ml of clean water at room temperature. Subsequently, 40 ml of ethanol was introduced into the reaction mixture. The reaction mixture was vigorously agitated until it reached a high viscosity within 30 min. TLC was employed to monitor the progress of the reaction. The outcome was subjected to filtration and rinsed with cold water, followed by recrystallization using 10 ml of ethanol. The product possesses the following physical characteristics: The stretching vibrations of orange FT-IR are as follows: 1701 cm⁻¹ for C=O, 1683 cm⁻¹ for C= N, 1530 cm⁻¹ for C=C, 3106 cm⁻¹ for C-H aromatic, and 2879 cm⁻¹ for C-H aliphatic. The ¹H NMR spectrum, recorded at 400 MHz in DMSO with a chemical shift (ε) in ppm, shows peaks at 6.84-7.68 (15 H, aromatic), 6.42 (1 H, C=CH), and 1.40 (3H, CH₃).

2.4 The general synthesis of 4-methyl-6-phenyl-6-(phenyl(phenylimino) methyl)-5,6-dihydropyrimidin-2(1*H*)-thione (compound A)

At room temperature (RT), a stirred solution of α , β -unsaturated ketone (1.0 mmol) dissolved in (10 ml) of ethanol was treated with a solution of thiourea (1.0 mmol) and glacial acetic acid (2.5 ml) [47–49]. The reaction mixture was refluxed for 24 h and heated to 80 °C. TLC was used to monitor the reaction's development. The product was recrystallized using ethanol as the solvent. Figure 1 elucidates the reaction equations. The results from the IR, (1 H and 13 C) NMR, and mass spectra all corresponded to the anticipated structure shown in Figs. 2, 3, 4, and 5. The physical properties of the product are brown; yield: 70%; M.p.:

Fig. 1 The equations of synthesis of compound A

155–157 °C; FT-IR stretching vibration v (cm⁻¹): 1550 (C=N), 1508 (C=C), 3063 (C–H aromatic), 2924 (C–H aliphatic), 3309 (N–H), 717.54 (C=S); ¹H NMR [400 MHz, DMSO, δ (ppm)]: 6. 13–7.933 (15 H, aromatic), 7.934 (1 H, N–H), 2.53 (3H, CH₃), 3.45 (2H, CH₂). ¹³ NMR [400 MHz, DMSO, δ (ppm)]: 39.67, 39.88, 40.09, 124.13, 126.80, 127.02, 127.19, 127. 41, 127.81, 128.76, 128.91, 129. 07, 130.00, 130.08, 182.92,183.47, 184.16, 195.33; mass, m/z: 387 (M⁺).

2.5 Experimental set-up

This study employed two cw laser beams for the Z-scan, DPs, and all-optical switching tests. The diameter of both beams as they exited the device's output couplers was 1.5 mm at e^{-2} . The wavelengths of these beams were 473 nm and 532 nm. A lens with a focal length of 5 cm was employed to focus the 473 nm beam into a spot measuring 19.235 µm, while the 532 nm beam was focused to spot measuring 21.635 um. The 473 nm beam is directed via two 20 cm focal length lenses to 76.941 µm, while the 532 nm beam is directed through the same lens to 86.539 µm. The Rayleigh lengths of the two beams are 2.456 mm and 2.363 mm for the 473 nm and 532 nm wavelengths, respectively. The procedures for building up an experimental Z-scan may be found in another source [28], and the processes for putting up an experimental DPs can also be found in another source [29].

In order to determine the NLRI, n_2 , and the nonlinear absorption coefficient (NLAC), β , it is necessary to conduct the Z-scan experiments where the transmittance is measured as a function of the sample position (±z). This experiment should be performed with both



2231 Page 4 of 22 J Mater Sci: Mater Electron (2024) 35:2231

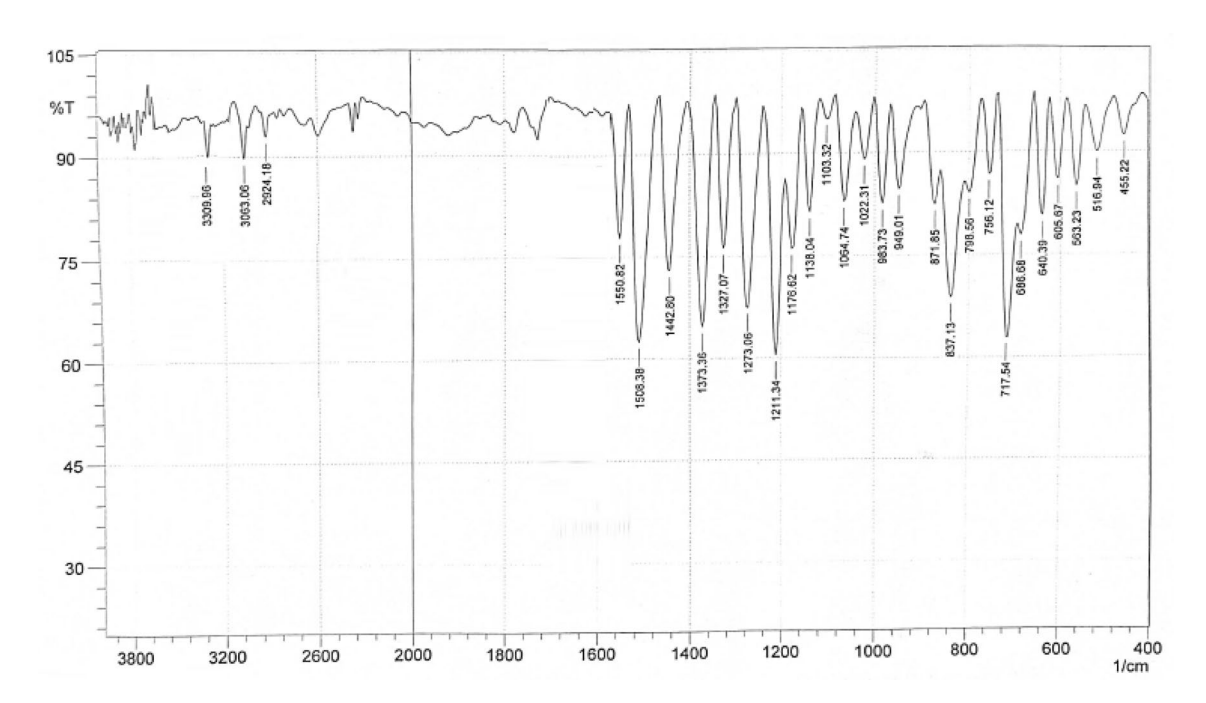
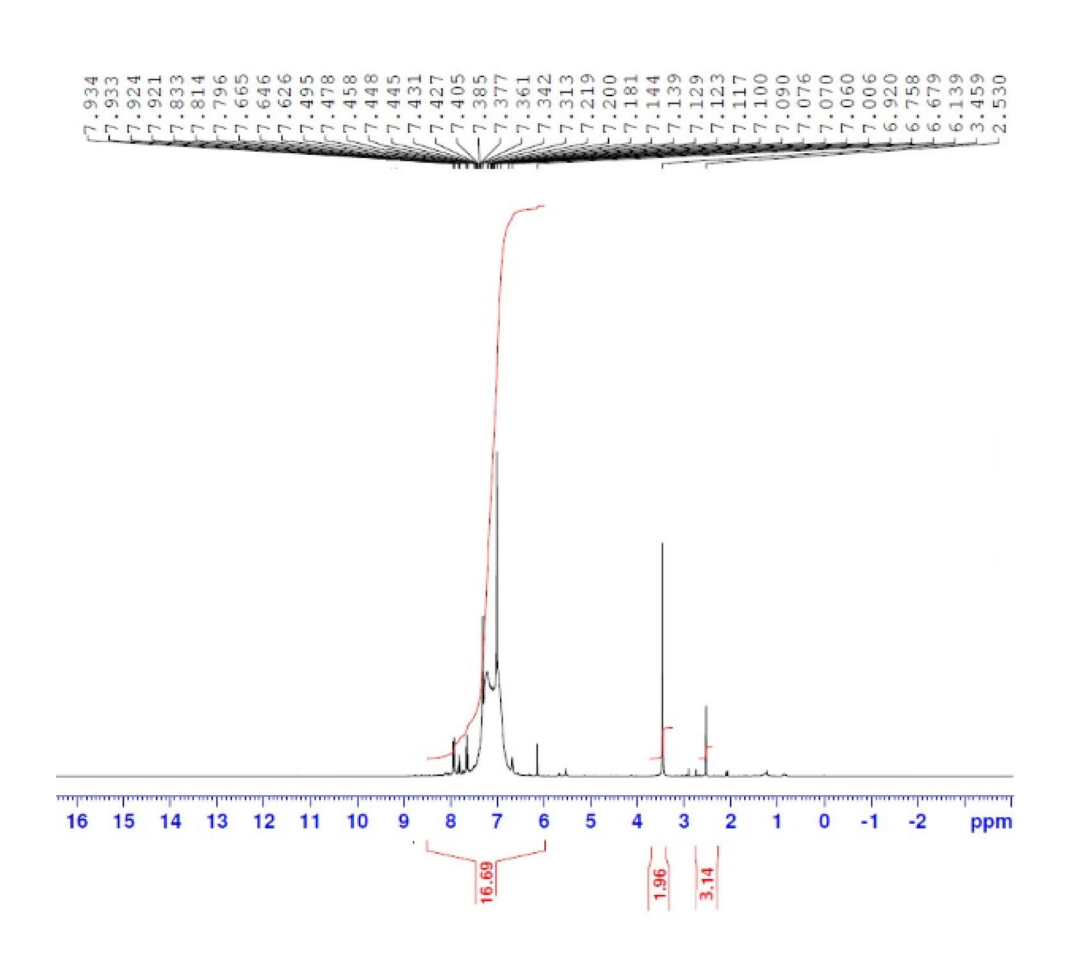
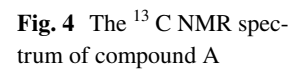


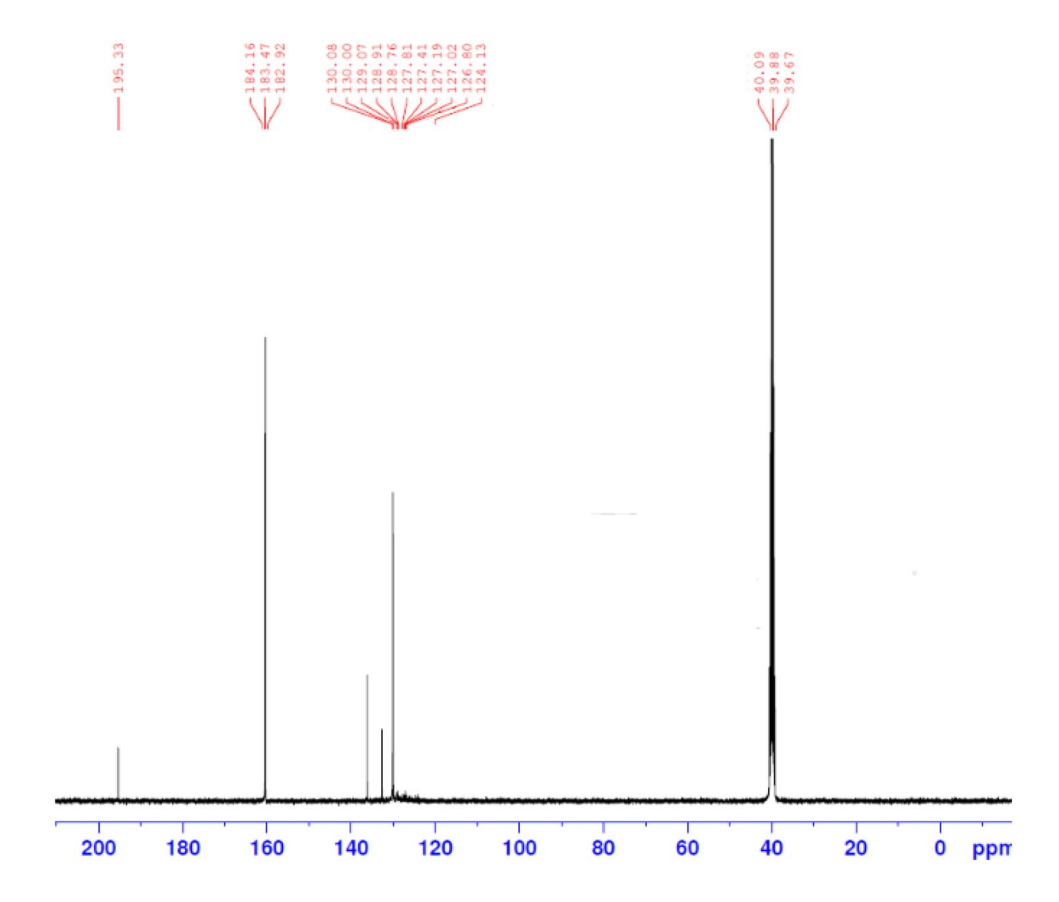
Fig. 2 The FT-IR spectrum of compound A

Fig. 3 The ¹H NMR spectrum of compound A









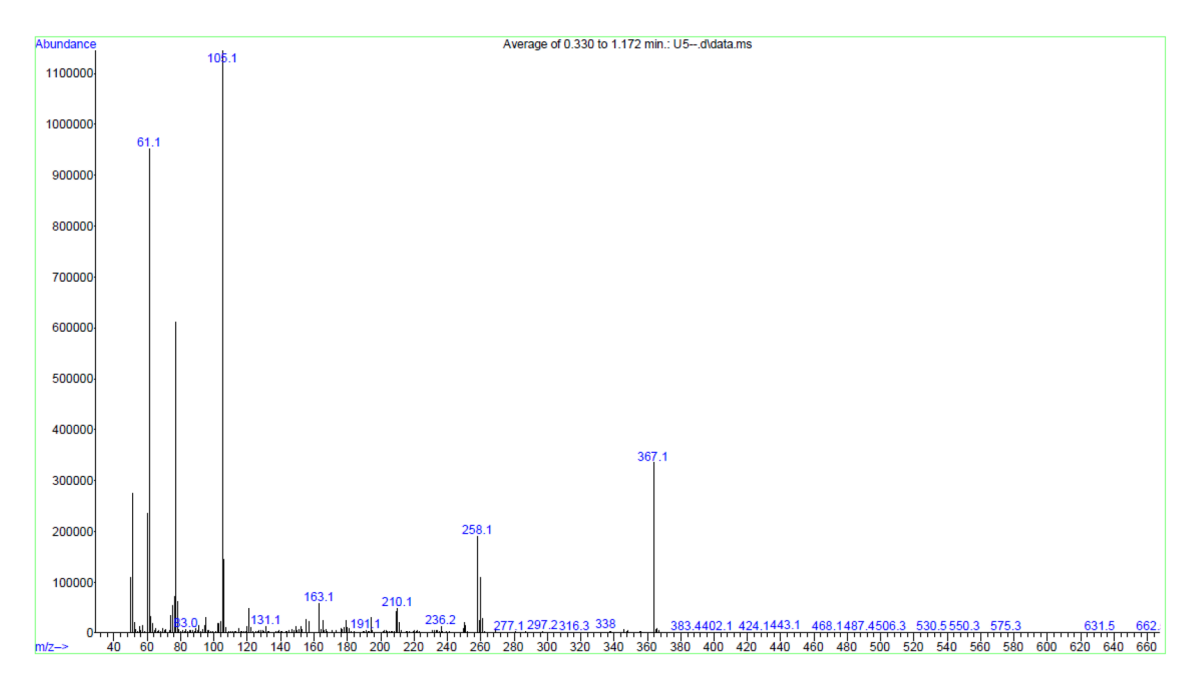


Fig. 5 The mass spectrum of compound A

2231 Page 6 of 22 J Mater Sci: Mater Electron (2024) 35:2231

closed and open apertures. The size of the DPs was determined by graphing the maximum number of DPs versus the power input.

3 Results

3.1 Chemistry

The reaction of imine compound containing $\alpha_{i}\beta_{i}$ unsaturated ketone with thiourea gave the corresponding dihydro pyrimidin-2(1H)-thione containing imine group derivative in good yield (Sect. 2). The resulted compound was brought in with a sharp melting point. The novel pyrimidine exhibited two distinct bands in the infrared spectra, both of which were associated with the imine moiety. There was a band observed at a wave number of 717.54 cm⁻¹ that correspond to the stretching of the (C=S) bond. Additionally, another band was observed at a wave number of 3309 cm⁻¹ that corresponds to the stretching of the (HN) bond. A peak corresponding to the stretching vibration of the (C=N) bond was observed in the spectrum at a wavenumber of 1550 cm⁻¹. The (C–H) aromatic band has peaks at approximately 3063 cm⁻¹, while the (C-H) aliphatic band showed peaks at 3309 cm⁻¹. The formation of these peaks can be attributed to the stretching vibrations of these bands.

The ¹H NMR spectrum of the novel compound, which was dissolved in DMSO, exhibited several signals originating from protons in aromatic rings, as well as an NH proton, within the chemical shift range of 6.13–7.93 ppm. Furthermore, a solitary signal emitted by protons in the (CH₃) group was detected at a chemical shift of 2.53 ppm. The spectrum exhibited a singlet signal within the 3.45 ppm region, originating from the protons in the CH₂ group of the pyrimidine ring. The ¹³C NMR signal validated the presumed structure of the synthesized molecule. The mass spectrum exhibited the molecular ion and other fragments that verified the structure of the synthesized medication.

3.2 UV-Visible spectrum

The absorbance spectrum of the compound A was stuided using UV–vis. spectrophotometer. Figure 6 represents the compound A absorbance spectrum. The compound A displayed an absorption peak at wavelength 230 nm belonging to electronic transitions π – π *. The value of the compound A linear absorption coefficient,

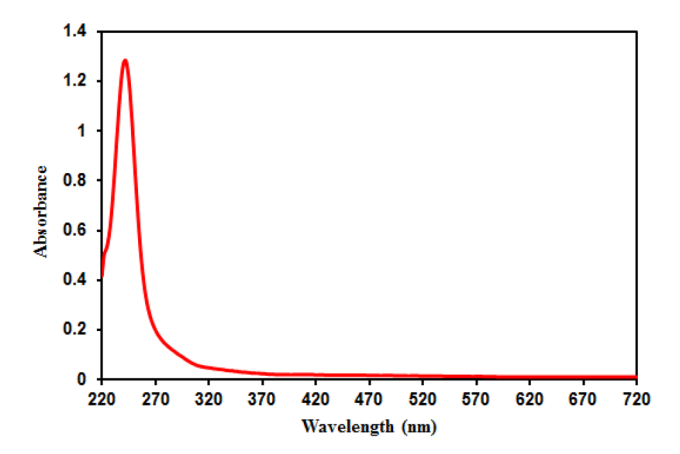


Fig. 6 Absorbance spectrum of compound A

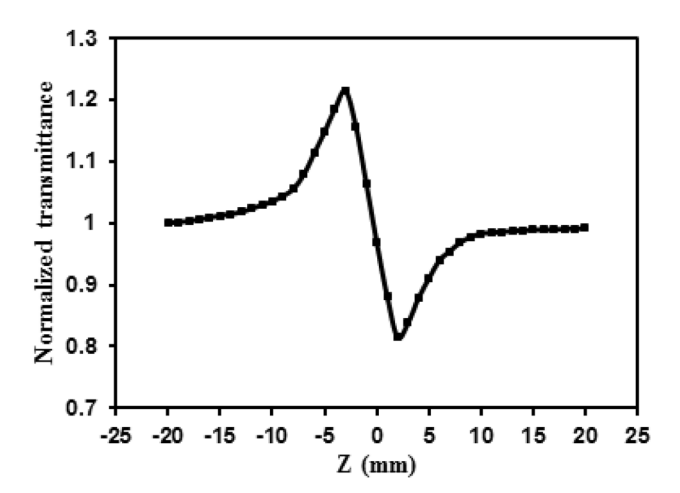


Fig. 7 CA Z-scan measurement result

 α , at wavelengths 473 nm and 532 nm is equal to 0.42 cm⁻¹ and 0.33 cm⁻¹, respectively, as it was determined using Fig. 6 and an equation given in [50].

3.3 Nonlinear study

The Gaussian laser beams were produced by two solid-state laser devices operating at wavelengths of 473 nm and 532 nm, with adjustable power ranging from 0 to 65 mW for the first device and 0 to 50 mW for the second device. The beams have radii of 1.5 mm as the beam emerges from the output coupler of the devices. The 473 nm wavelength was employed for the Z-scan and DPs.

The consequence of the CA Z-scan measurements is depicted in Fig. 7 for the compound A where the normalized transmittance is drawn against the sample position (±z) relative to beam focus. Figure 7 shows a



peak and then a valley, which proves that the sample has a negative NLRI, and in other words, the occurrence of self-defocusing. While OA Z-scan measurements showed a straight horizontal line, which indicates that the compound A does not have a NLAC. The Z-scan measurements were conducted with a power input of 5 mW, resulting in an intensity of 688.8 W/cm². The utilization of a cw laser beam leads to the generation of heat, which in turn causes the nonlinearity seen by compound A.

In the DPs experiments, the results of effect of power input on the DPs and the beam wave front on the DPs are shown in Figs. 8 and 9, respectively. When the power input increased, the sample absorbed more energy due to the large absorption coefficient so that more heat resulted due to the radiation-less transitions. The negative lens effect occurs due to the Gaussian dispersion of the laser beam, which leads to the production of heat. As depicted in Fig. 8, the beam that was sent out initially traced a little circular spot on the far screen. Subsequently, it fragmented into distinct rings, with the quantity of rings progressively increasing until an irregular pattern emerged. This is due to the greater increase in the thermal vertical convection current compared to the thermal horizontal conduction current. When choosing two types of beam wave fronts, two types of DPs appeared, an effect noticed as early as 1984 by Santamato et al. [51–53] as seen in Fig. 9. The behavior observed in Fig. 8 is analogous to that depicted in Fig. 10, which illustrates the temporal evolution of a selected data point. Figure 10 illustrates

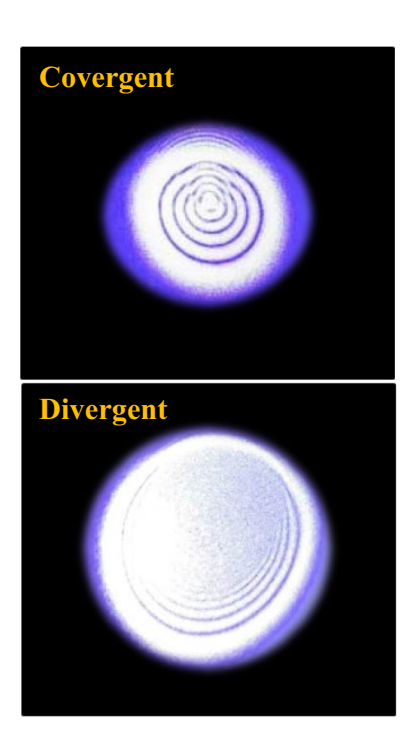
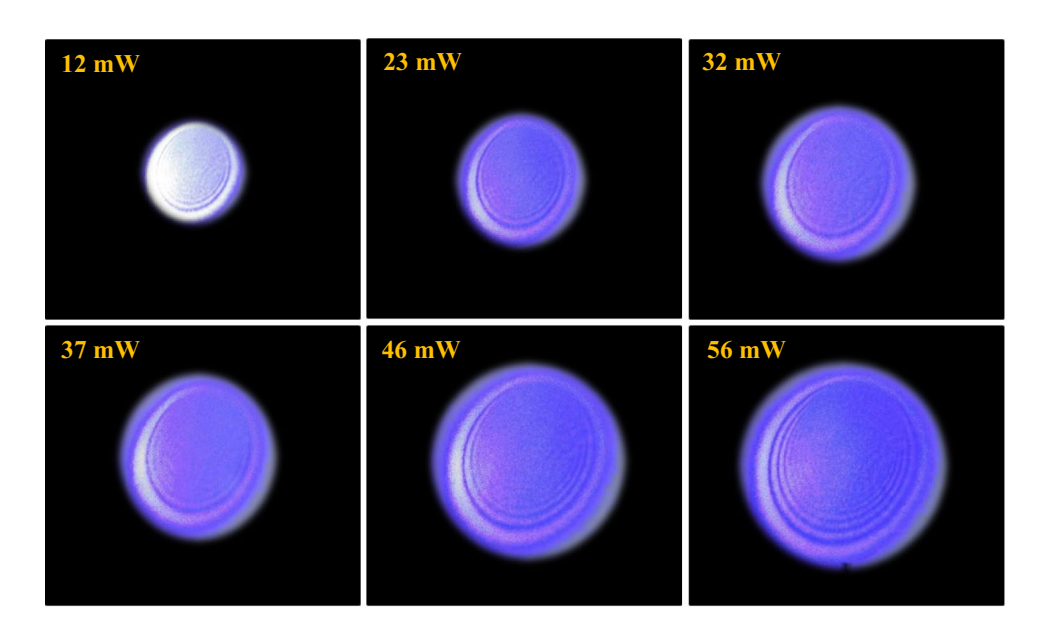


Fig. 9 Laser beam wave front effect at 56 mW DPs in compound A

the temporal variation of the selected DP under the influence of a power input of 56 mW on compound A.

The controlling beam for all-optical switching utilizes a laser beam with a wavelength of 473 nm. The medium exhibits a significantly high absorption coefficient, indicating its ability to readily absorb a substantial amount of energy. This facilitates the process of

Fig. 8 Power input effect of the DPs obtained in compound A





2231 Page 8 of 22 J Mater Sci: Mater Electron (2024) 35:2231

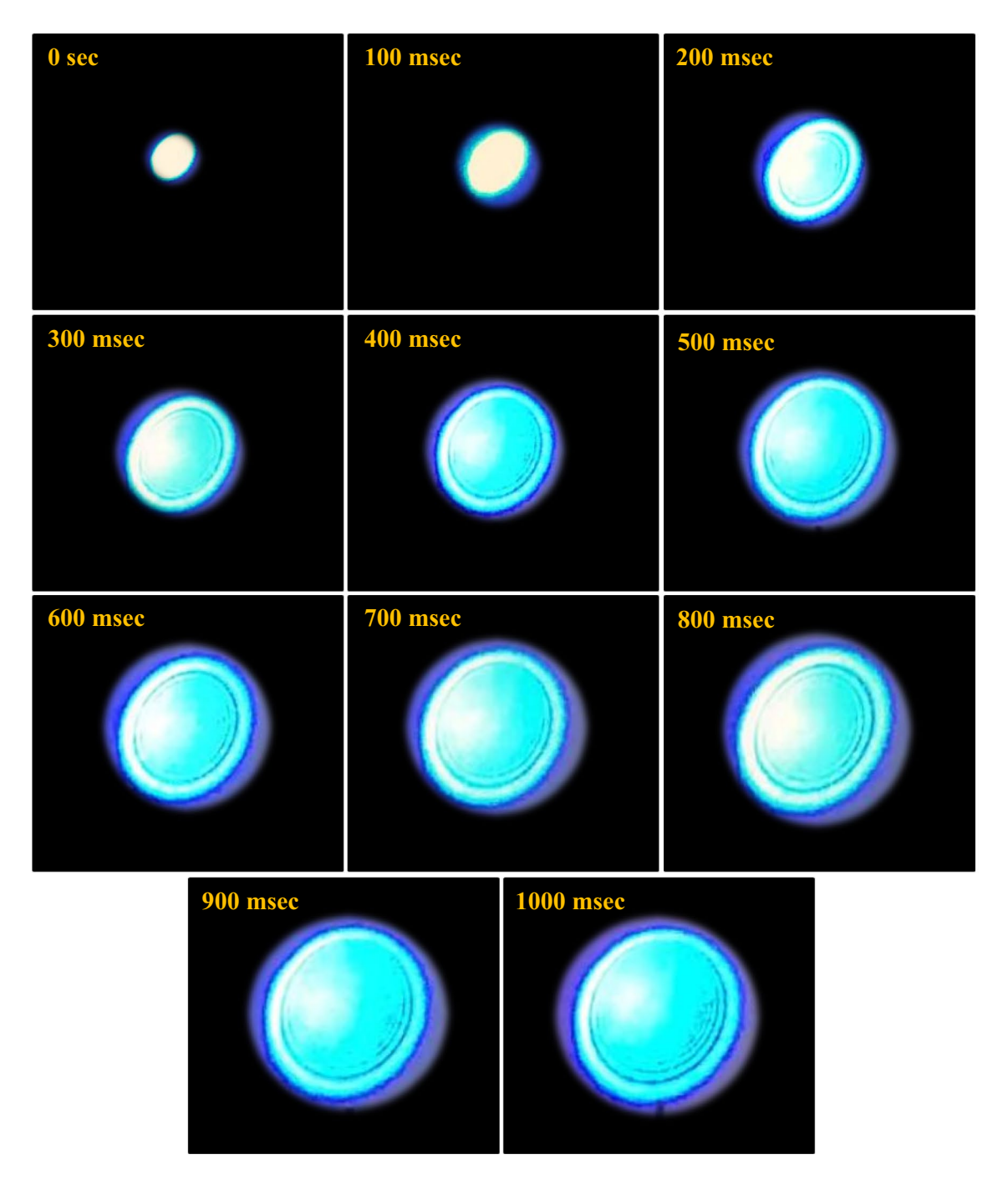


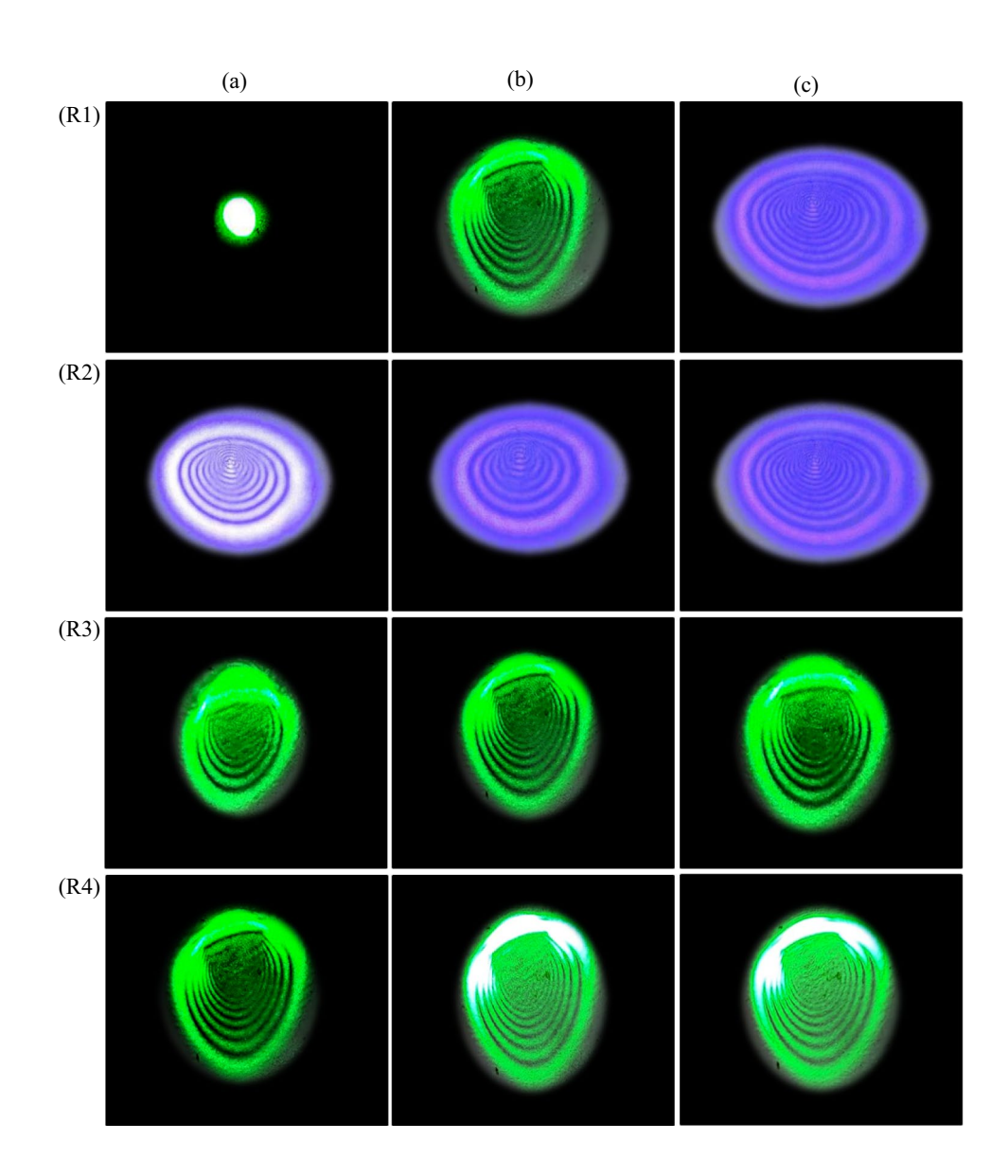
Fig. 10 Temporal evolution of a chosen DP at 56 mW in compound A

creating a DP. The device is manipulated by an alternate beam that has a wavelength of 532 nm. Due to its low absorption coefficient, the medium receives only a minimal quantity of energy, resulting in the absence of any detectable DPs. The x-passing approach allows for simultaneous passage of both beams through the medium. This results in the formation of two distinct types of DPs: one induced by the controlling beam

and another induced by the controlled beam. This phenomenon is attributed to cross-self-phase modulation (XSPM) [54–56]; as presented in Fig. 11, both beams are of cw behavior, while in Fig. 12 controlling beam is of pulsed behavior where the laser head was connected to the TTL function of a frequency generator, while the controlled one was of cw behavior.



Fig. 11 cw or static AOS in the compound A



3.4 Calculation of the NLRI due to

3.4.1 Z-scan

Since the origin of nonlinearity in the compound A is thermal, the NLRI, n_2 , due to the Z-scan can be determined from the following equation [57, 58]

$$n_2 = \frac{\Delta T_{\text{p-v}} \lambda}{4\pi dI},\tag{1}$$

where λ represents the wavelength of the laser beam, d refers to the thickness of the sample, and $\Delta T_{\rm p-v}$ denotes the transmittance difference between the peak and valley. Equation 1 was employed to calculate the NLRI of the compound A, so that it equals to $0.21 \times 10^{-7}~{\rm cm^2/W}$ at an intensity of 688.28 W/cm².

3.4.2 *DPs*

Considering the fact that thermal change of the medium RI, Δn , NLRI is expressed as $\Delta n = n_2 I$ and $I = \frac{2P}{\pi \omega^2}$. The expression for n_2 can be derived by Eq. (2) [59]

$$n_2 = \frac{\pi \omega_0^2}{2n_0 d} \frac{N}{P} \tag{2}$$

 ω_0 is the beam radius, n_0 is the medium linear RI, so that for N=8, P=56 mW, I=9640 W/cm², d=1 mm, $\lambda=473$ nm, $n_0\sim 1$, $\omega_0=19.235$ μ m, so that $n_2=43.925\times 10^{-7}$ cm²/W.



2231 Page 10 of 22 J Mater Sci: Mater Electron (2024) 35:2231

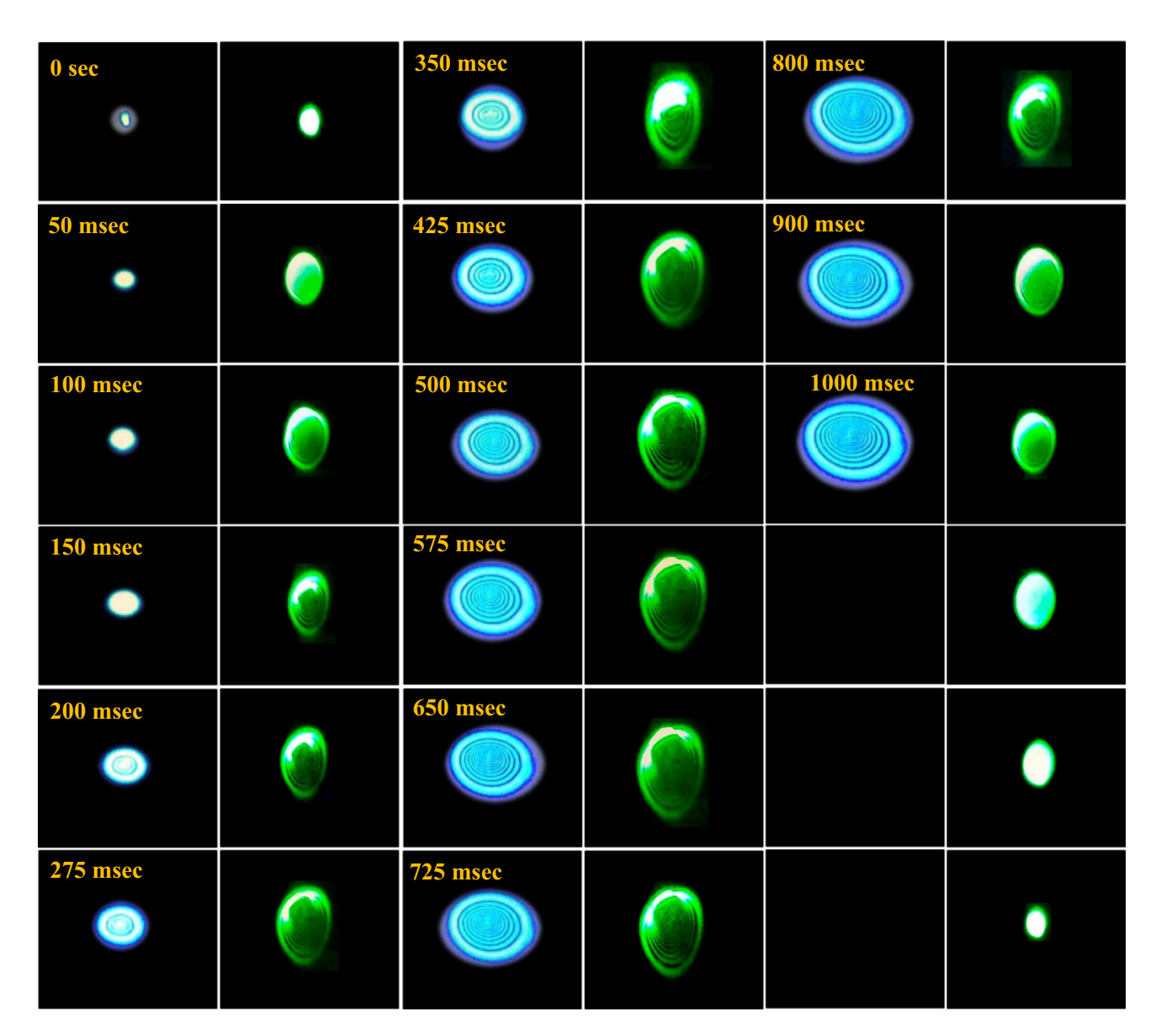


Fig. 12 Pulsed or dynamic AOS in compound A

3.5 Simulating the DPs numerically

The passage of a certain laser beam through a medium can lead to the rise of the medium temperature due to the absorption of part of the beam energy that followed with radiation-less transitions. As a result, the medium RI changes, that lead to the change of the beam phase. Following the procedure of Karimzadeh [60], the DPs resulted on the screen situated at a distance L in the far field can be obtained using the following equation

$$I(x',y',t) = \left| E_0 \frac{i\pi\omega^2}{\lambda L} \exp(ikL) \exp\left(-\frac{\alpha d}{2}\right) \int_{-\infty}^{\infty} dx \int_{-\infty}^{\infty} dy \right|$$

$$\times \exp\left(-\frac{x^2 + y^2}{\omega^2}\right) \cdot \exp\left[\left\{-k\frac{x^2 + y^2}{2R} + \Delta\varphi(x,y,t)\right\}\right] \cdot \exp\left(-ik\frac{xx' + yy'}{L}\right) \right|^2$$
(3)



where E_0 is the beam field, k is the beam propagation vector, α is the medium absorption coefficient, ω is the beam radius at e^{-2} , R is beam wave front radius, and $\Delta \varphi$ is the change of the beam phase as a result of passing through the sample. The solution of Eq. (3) numerically led to the results shown in Figs. 13, 14, 15, 16, 17, 18, 19, 20, 21, and 22. Figures 13, 14, and 15 show the simulation results of the results given in Figs. 8, 9, and 10 where good accord can be seen. For more results, Figs. 16, 17, and 18, the variation of the beam phase as it traverse the sample and the variation of the sample temperature, spatially respectively, the results are shown in Figs. 19, 20 and 21, together with their behavior under the variations of beam wave front and variations of the light intensity against x and y axes. Figure 22 displays direct comparison between experimental (blue) and numerical (red) results when it can be seen good accord among both.

4 Conclusion

A molecule with a 5,6-dihydro pyrimidin-2(1*H*)-thione (compound A) structure and an imine group was synthesized and characterized. The proposed structure of

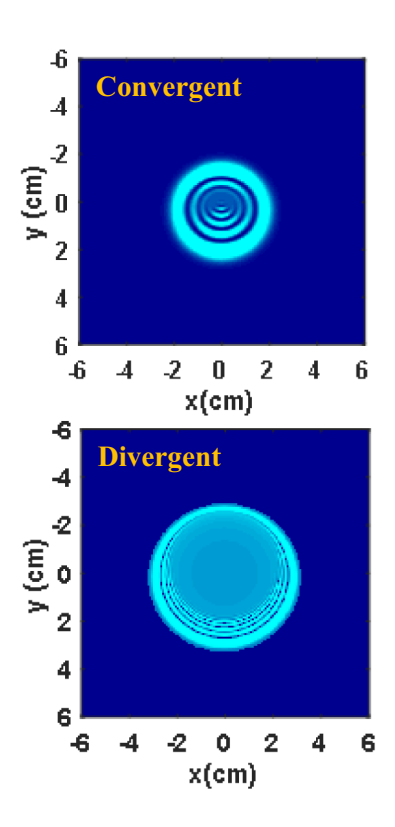


Fig. 14 Simulation of wave front dependence of DPs in compound A

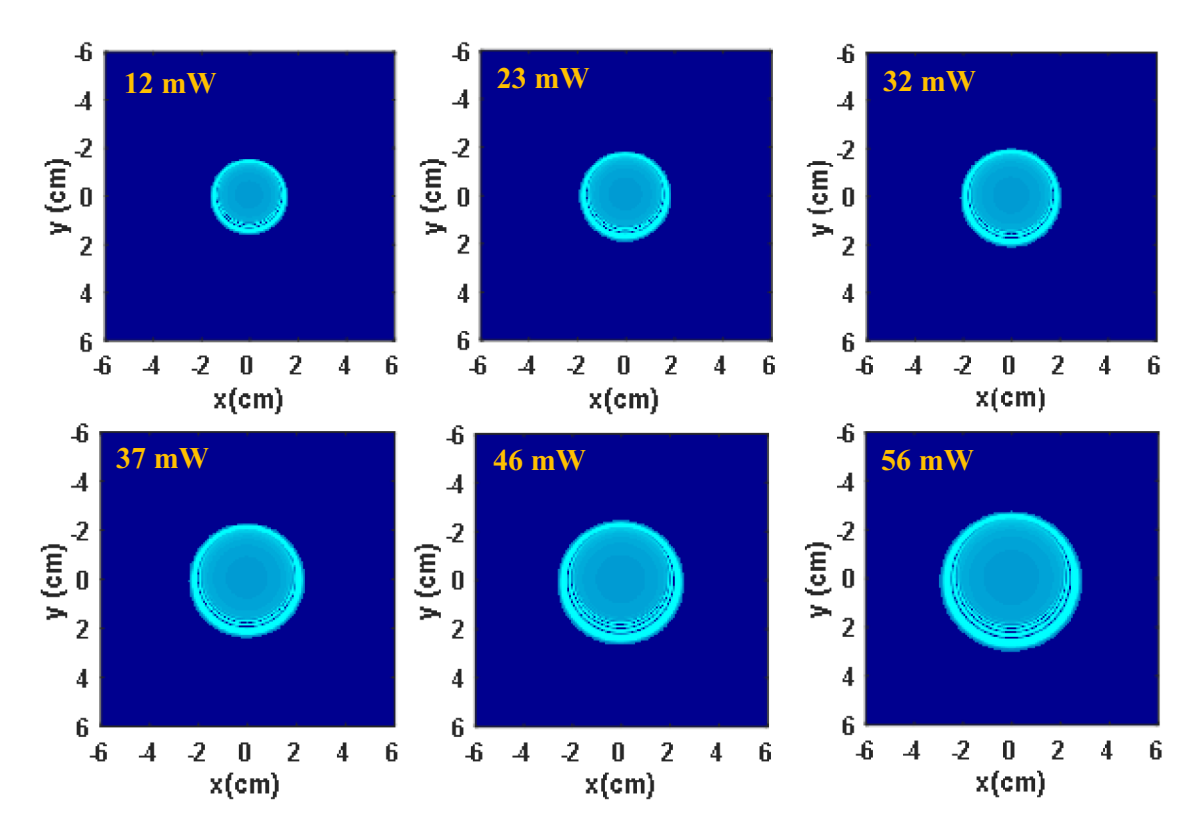


Fig. 13 Simulation of power input dependence of DPs in compound A



2231 Page 12 of 22 J Mater Sci: Mater Electron (2024) 35:2231

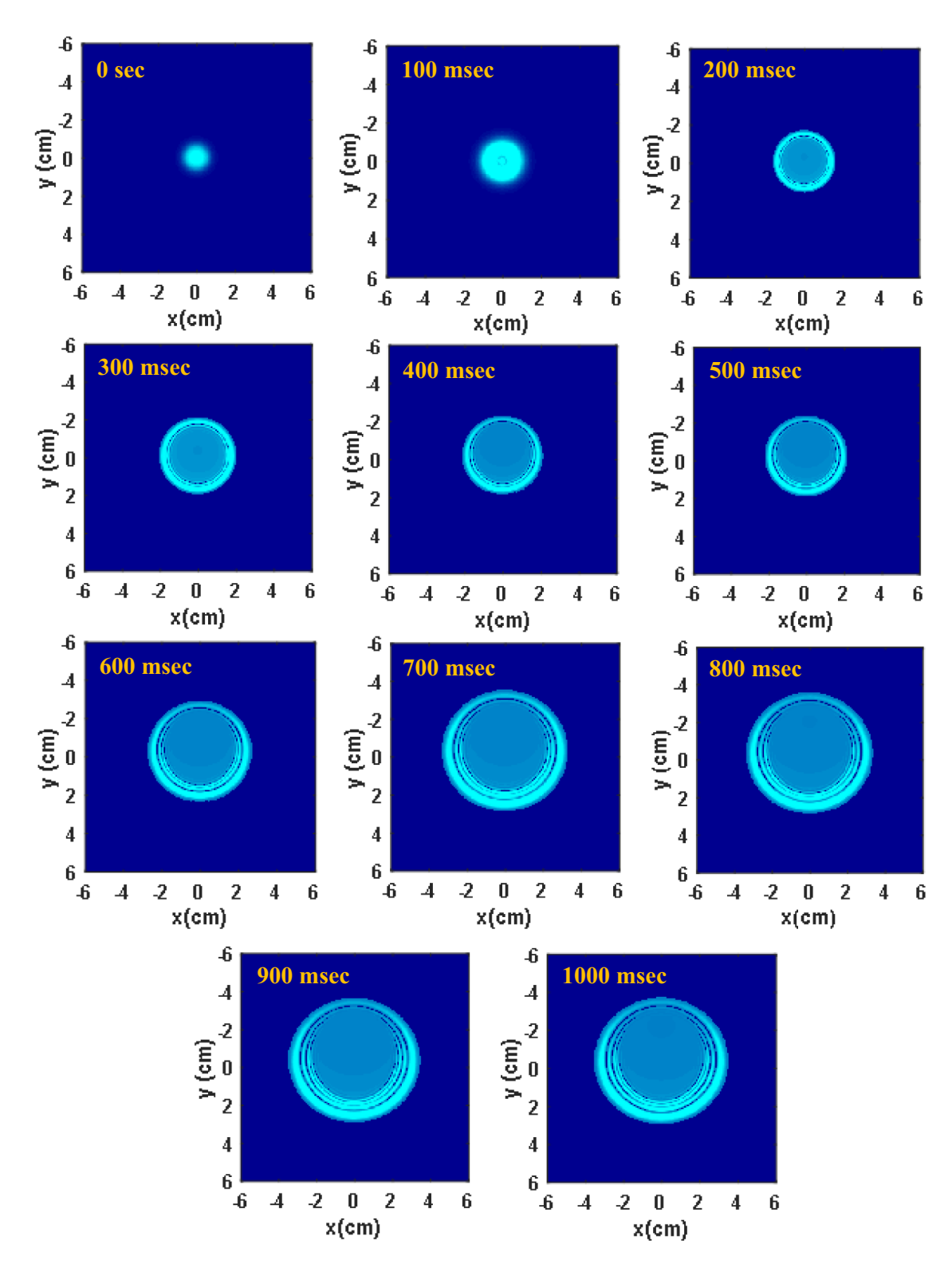
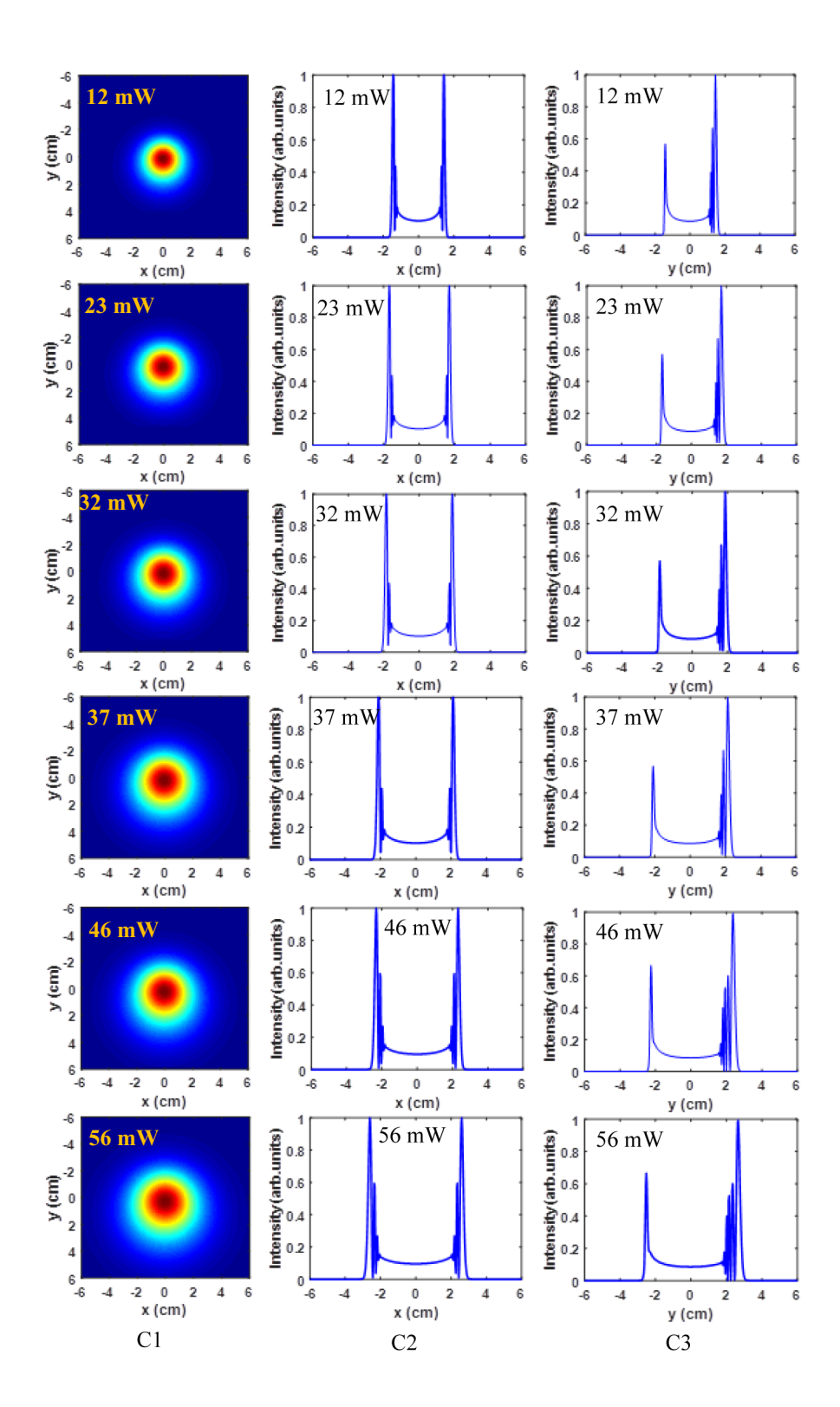


Fig. 15 Simulation of temporal evolution of DPs in compound A



Fig. 16 Simulation of (C1) beam phase for the power input mW shown of (C2) intensity variation with power input against *x* axis and (C1) intensity variation with power input against *y* axis, all in compound A





2231 Page 14 of 22 J Mater Sci: Mater Electron (2024) 35:2231

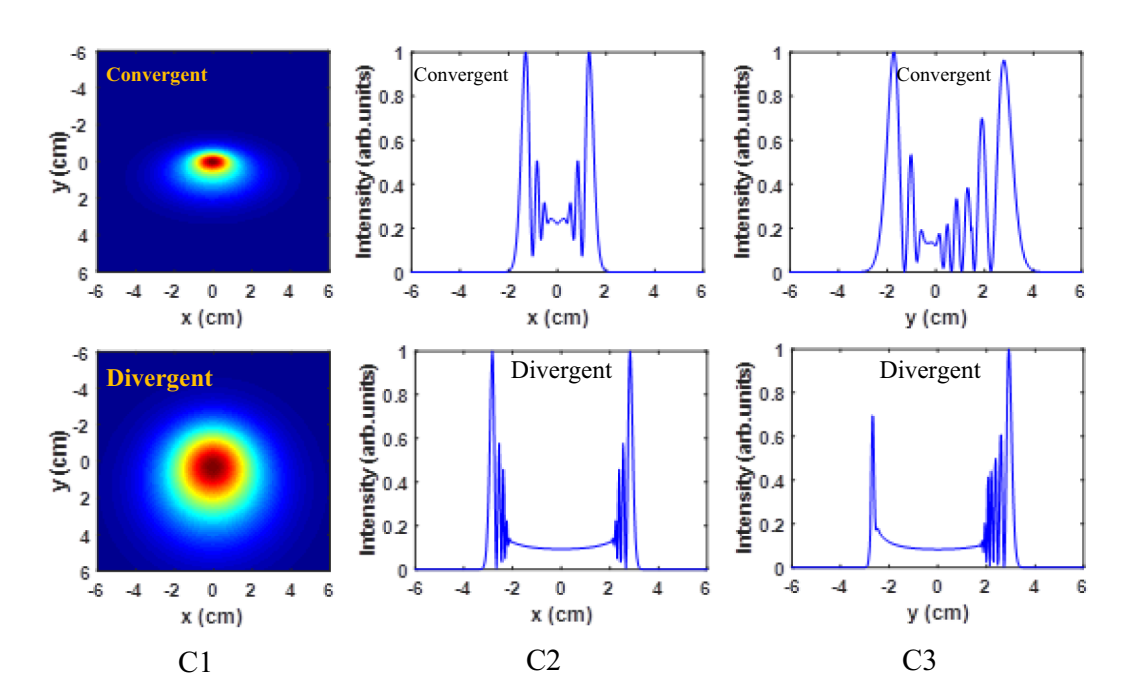


Fig. 17 Same as Fig. 16 with effect of beam wave front (C1) beam phase (C2) intensity against x axis and (C3) intensity against y axis in compound A

the synthesized molecule was confirmed by analyzing its infrared spectrum, nuclear magnetic resonance spectrum (¹H and ¹³C), and mass spectrometry's data. Moreover, this new chemical exhibit stability in the presence of moisture and light. The Z-scan and DPs were produced due to the alteration of the beam wave

front caused by the passage of a continuous 473 nm laser beam through the compound A. The nonlinear refraction index (NLRI) was calculated to be 0.21×10^{-7} cm²/W and 3.925×10^{-7} cm²/W, respectively, using both techniques. The DPs were numerically calculated using the Fresnel-Kirchhoff integral.



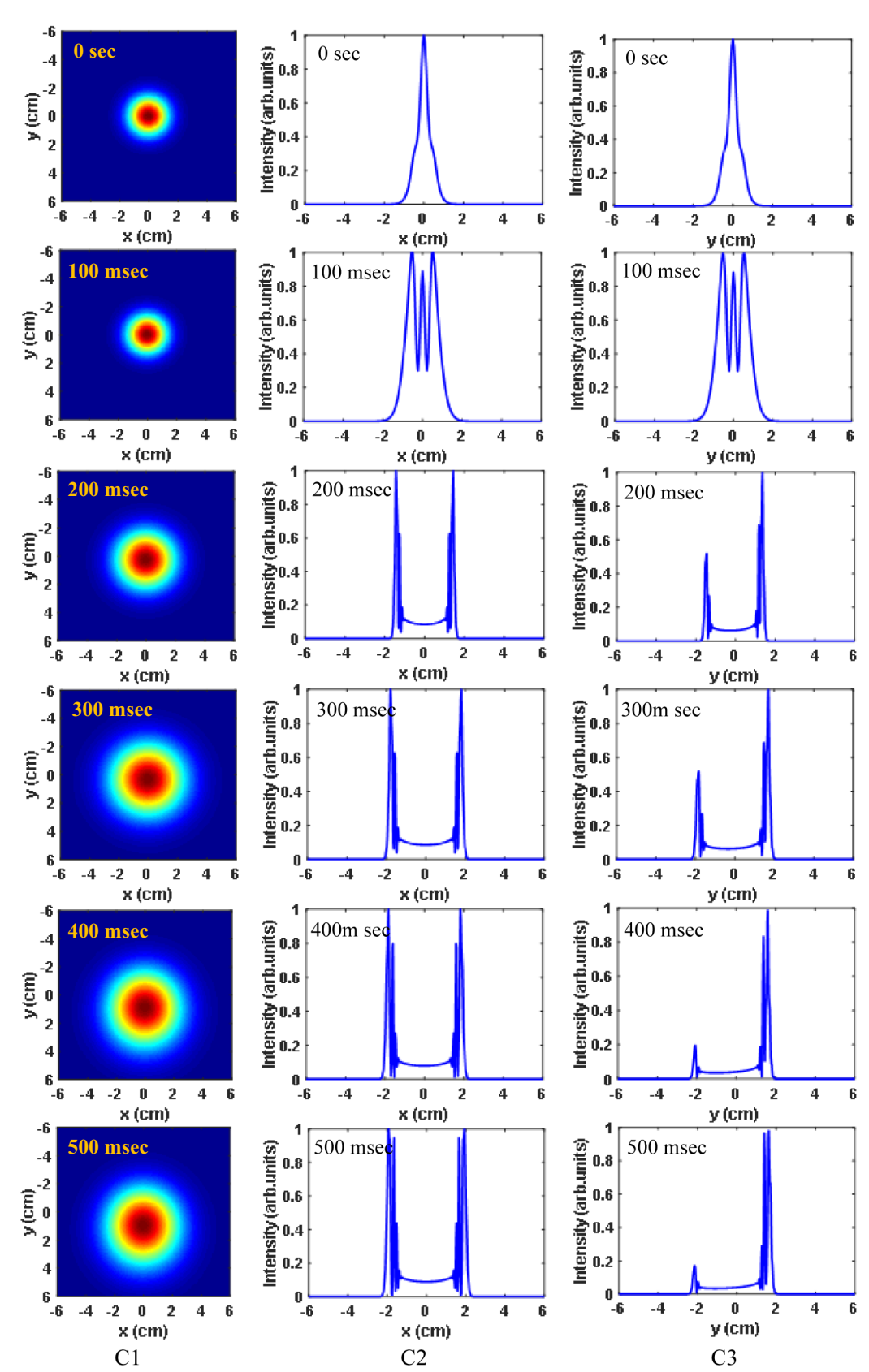


Fig. 18 Simulation of (C1) temporal behavior beam phase, of (C2) and (C3) beam intensity against x axis and y axis, respectively, in compound A



2231 Page 16 of 22 J Mater Sci: Mater Electron (2024) 35:2231

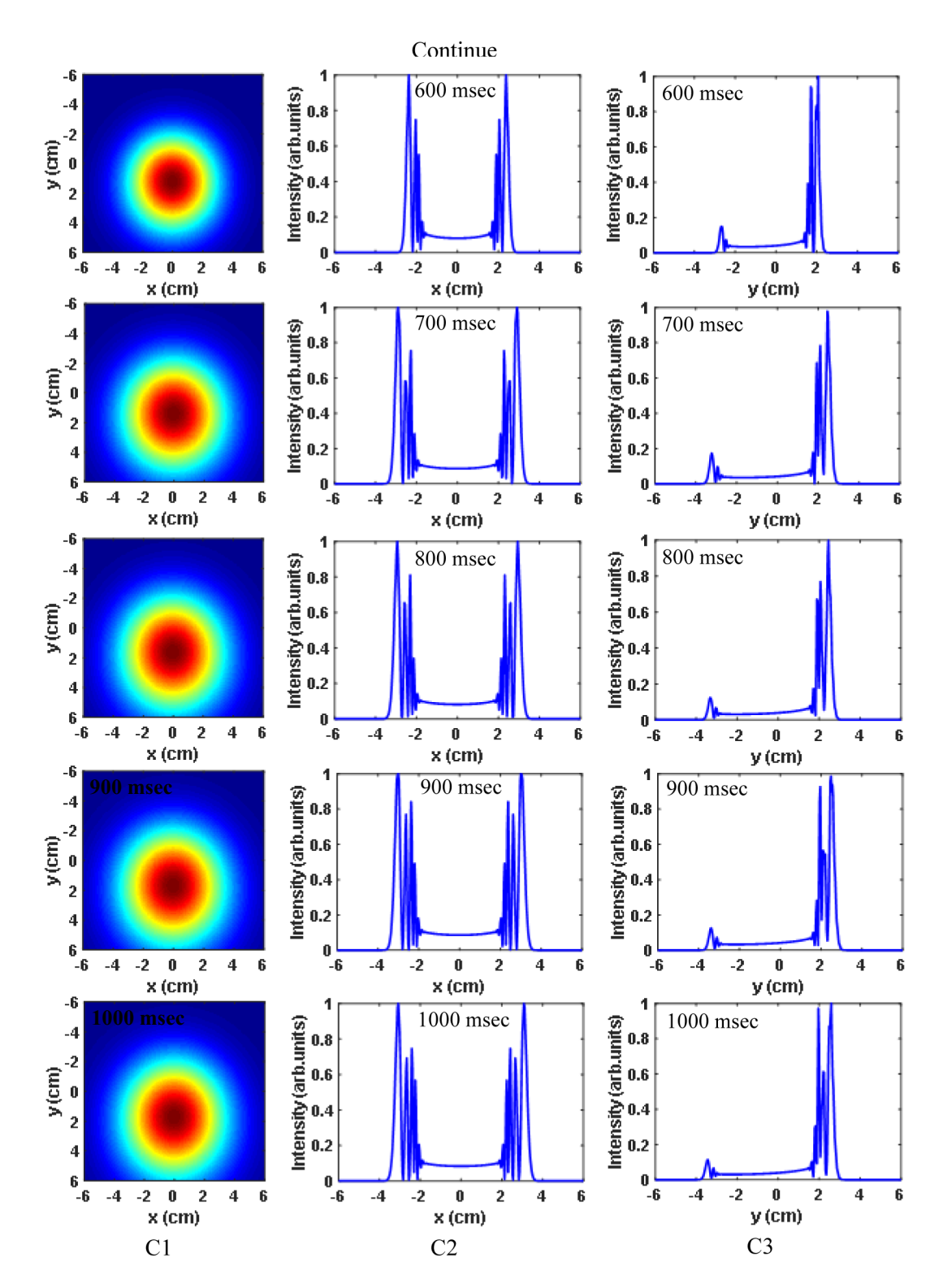


Fig. 18 continued



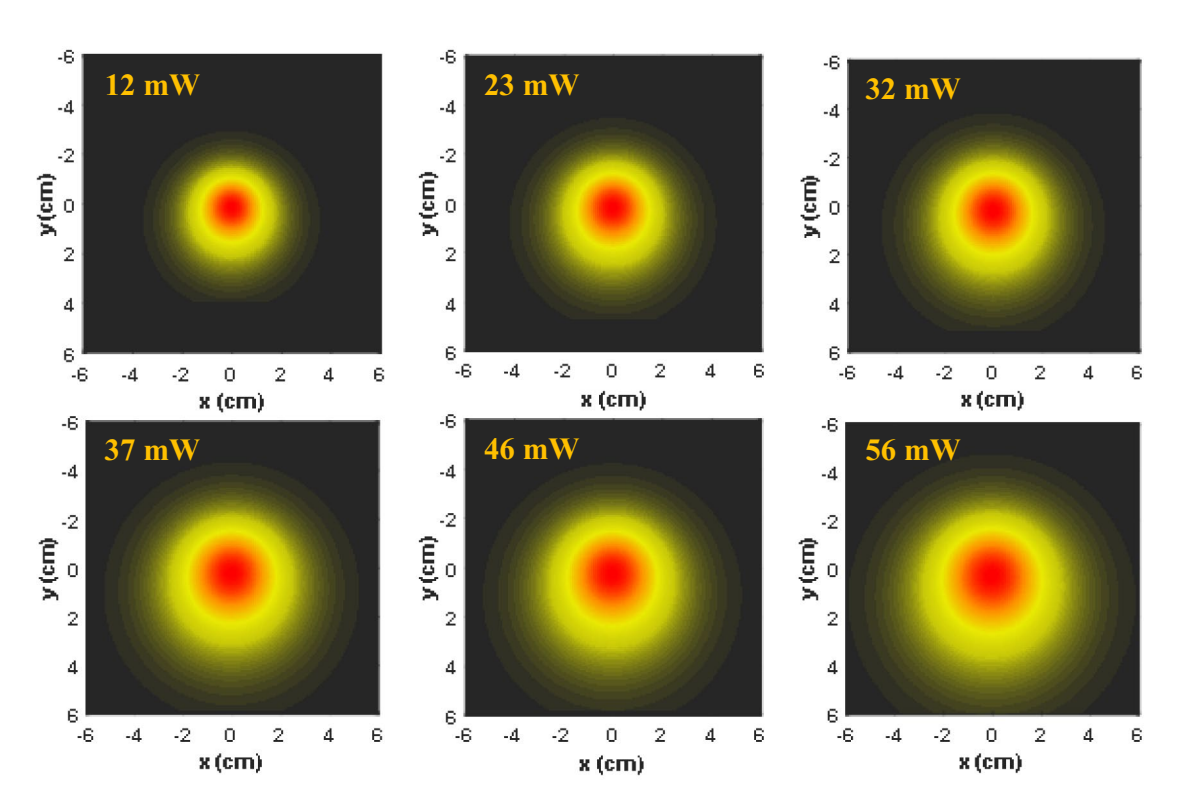
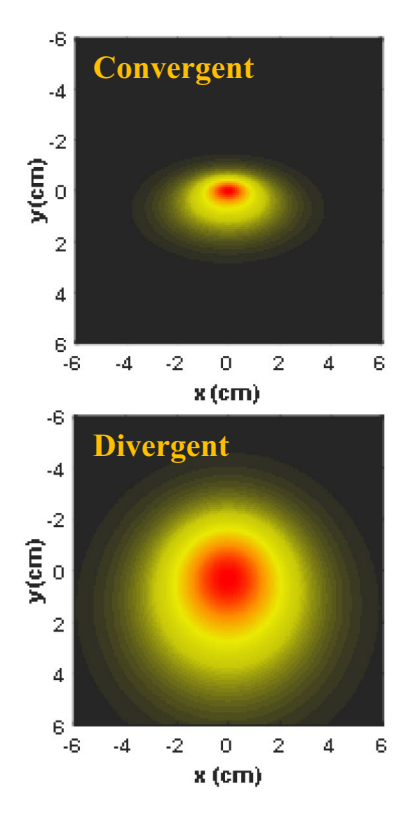


Fig. 19 Simulation of medium temperature against power input in compound A



 $\label{eq:Fig.20} \textbf{Fig. 20} \ \ \text{Simulation of medium temperature against wave front in compound A}$



2231 Page 18 of 22 J Mater Sci: Mater Electron (2024) 35:2231

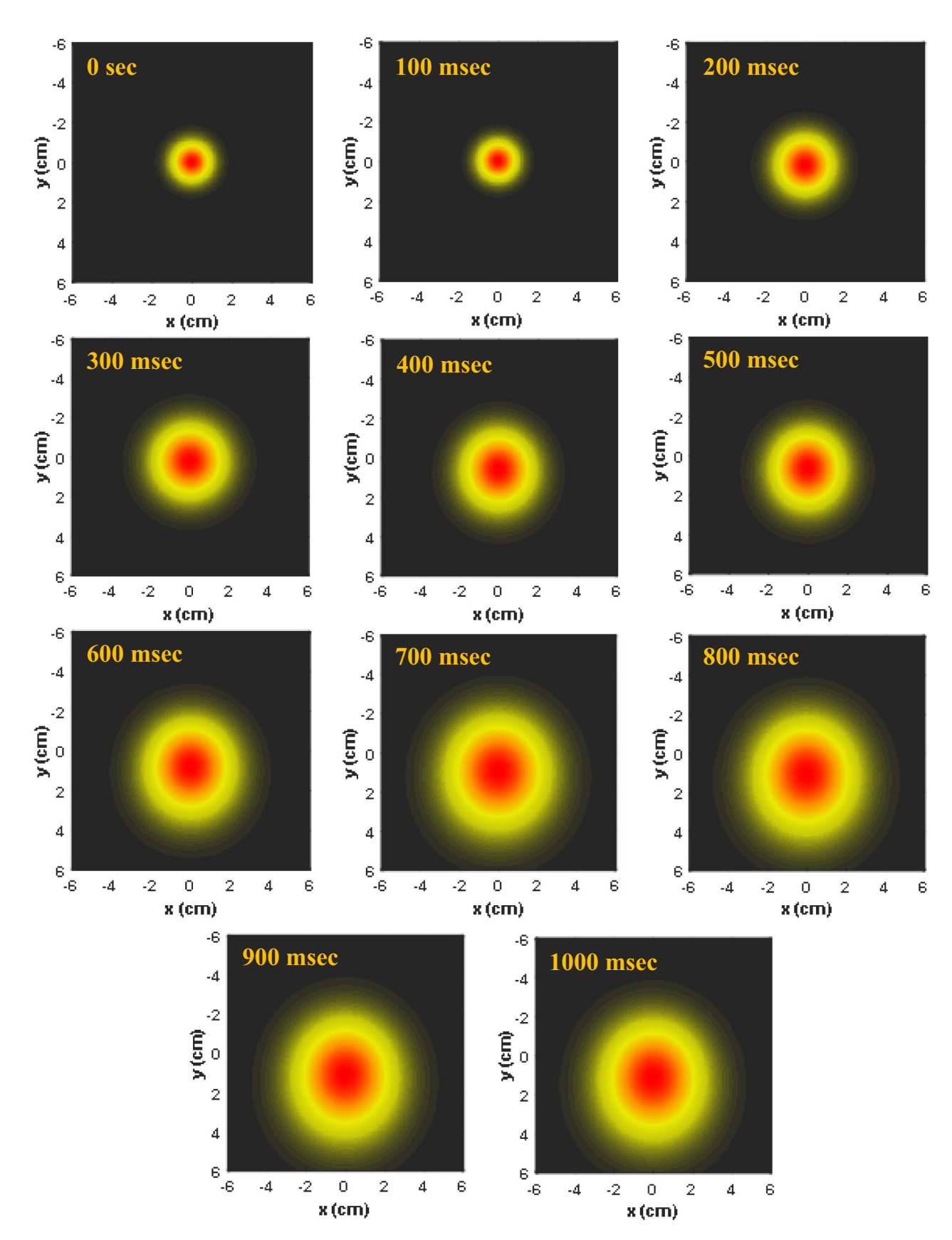


Fig. 21 Simulation of medium temperature temporal variation in compound A



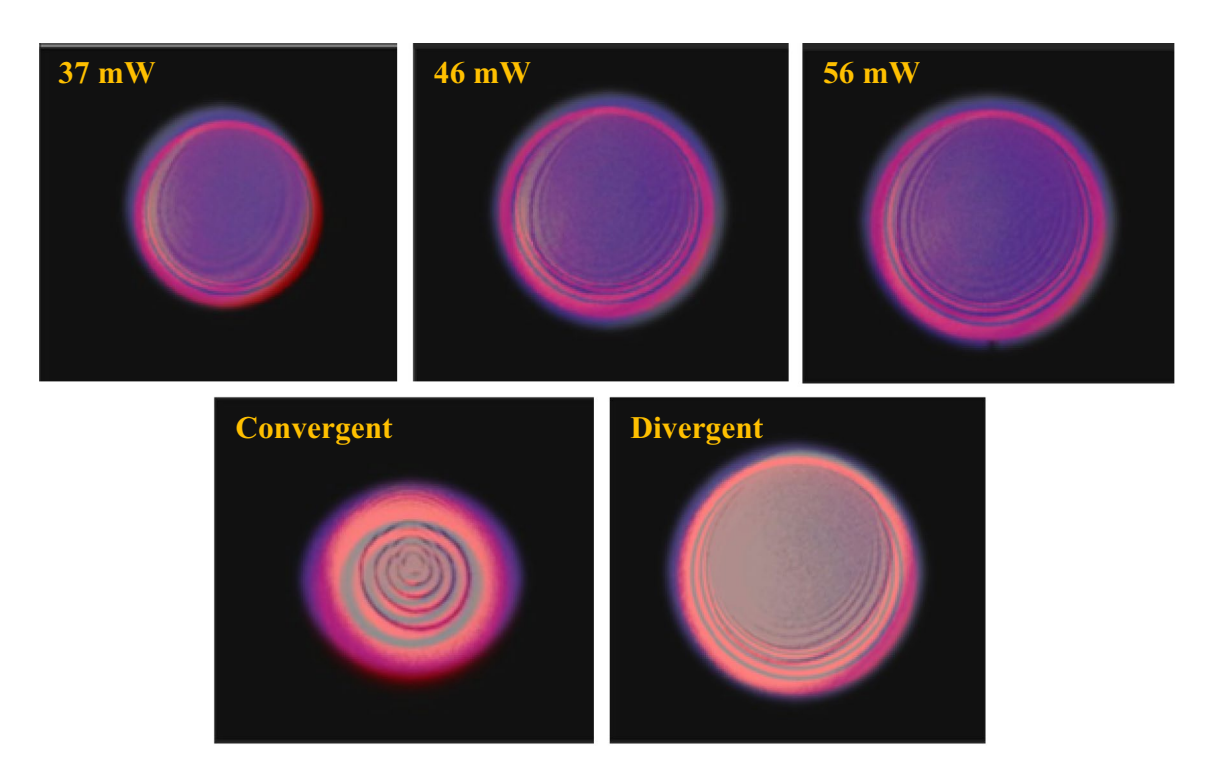


Fig. 22 Comparison of experimental results (blue) and simulation ones (red) in compound A (Color figure online)

Author contributions

Jenan Al Ameri synthesized the compound, H. A. Sultan and Mariam Abdul-Bary participated in the characterization and analysis of the results, Qusay M.A. Hassan and Batool Haddad wrote the main manuscript, and C. A. Emshary wrote the main manuscript text—review and editing. All authors reviewed the manuscript.

Funding

The authors have not received any funding.

Data availability

The authors confirm that the data supporting the findings of this study are available within the article.

Declarations

Competing interests The authors declare that they have no known competing financial interests or per-

sonal relationships that could have appeared to influence the work reported in this paper.

Ethical approval and Consent to participate The authors declare that their commitment to ethics related to his work and they have designed the experiments, collected and analyzed the data, and written the manuscript.

Consent for publication The authors declare their consent of publication.

References

- Kh.A. Al-Timimy, Q.M.A. Hassan, H.A. Sultan, C.A. Emshary, Solvents effect on the optical nonlinear properties of the Sudan IV. Optik 224, 165398 (2020)
- C.A. Emshary, Q.M.A. Hassan, H. Bakr, H.A. Sultan, Determination of the optical constants, nonlinear optical parameters and threshold limiting of methyl red-epoxy resin film. Phys. B 622, 413354 (2021)
- S.A. Ali, Q.M.A. Hassan, C.A. Emshary, H.A. Sultan, Characterizing optical and morphological properties of Eriochrome Black T doped polyvinyl alcohol film. Phys. Scr. 95, 095814 (2020)



2231 Page 20 of 22 J Mater Sci: Mater Electron (2024) 35:2231

- C.A. Emshary, I.M. Ali, Q.M.A. Hassan, H.A. Sultan, Linear and nonlinear optical properties of potassium dichromate in solution and solid polymer film. Physica B 613, 413014 (2021)
- Q.M.A. Hassan, C.A. Emshary, H.A. Sultan, Investigating the optical nonlinear properties and limiting optical of eosin methylene blue solution using a CW laser beam. Phys. Scr. 96, 095503 (2021)
- D. Sinha, T. Swu, S.P. Tripathy, R. Mishra, K.K. Dwived,
 D. Fink, Gamma-photon induced modifications in polyvinylchloride (PVC) film. Radiat. Eff. Defects Solids 158, 593–598 (2003)
- J.H. Jebur, Q.M.A. Hassan, M.F. Al-Mudhaffer, A.S. Al-Asadi, R.S. Elias, B.A. Saeed, C.A. Emshary, The gamma radiation effect on the surface morphology and optical properties of alphamethyl curcumin: PMMA film. Phys. Scr. 95, 045804 (2020)
- G. Santhosh, B.S. Madhukar, G.P. Nayaka, B.C. Hemaraju, B. Siddaramaiah, Influence of gamma radiation on optical properties of Halloysite nanotubes incorporated polycarbonate nanocomposites. Radiat. Eff. Defects Solids 17, 489–503 (2018)
- SSh. Fleifil, Q.M.A. Hassan, A.M. Dhumad, H.A. Sultan, C.A. Emshary, Gamma radiation effect on the optical linear and nonlinear properties of PVA with trypan blue film. Radiat. Effects Defects Solids 178, 699–723 (2023)
- A. Badawi, S.J. Alsufyani, S.S. Alharthi, M.G. Althobaiti, A.A. Alkathiri, M. Almurayshid, A.N. Alharbi, Impact of gamma irradiation on the structural, linear and nonlinear optical properties of lead oxide incorporated PVA/graphene blend for shielding applications. Opt. Mater. 127, 112244 (2022)
- A.M. Jassem, Q.M.A. Hassan, C.A. Emshary, H.A. Sultan, F.A. Almashal, W.A. Radhi, Synthesis and optical nonlinear properties performance of azonaphthol dye. Phys. Scr. 96, 025503 (2021)
- Q.M.A. Hassan, H.A. Sultan, A.S. Al-Asadi, A.J. Kadhim, N.A. Hussein, C.A. Emshary, Synthesis, characterization, and study of the nonlinear optical properties of two new organic compounds. Synth. Met. 257, 116158 (2019)
- J. Priscilla, G.V. Vijayaraghavan, K. Yukesh Kumar, Influence of procion red dye doping on the structural, dielectric and optical properties of diglycine-phthalic acid single crystals for nonlinear optical applications. J. Mater. Sci. Mater. Electron. 35, 1265 (2024)
- Q.M.A. Hassan, N.A. Raheem, C.A. Emshary, A.M. Dhumad, H.A. Sultan, T. Fahad, Preparation, DFT and optical nonlinear studies of a novel azo-(β)-diketone dye. Opt. Las. Technol. 148, 107705 (2022)

- R. Sivaranjani, A. Suvitha, N. Alharbi, T. Arumanayagam, Experimental and DFT perspectives: exploring spectral, linear and nonlinear optical properties of p-nitrophenol complex crystal for NLO applications. J. Mater. Sci. Mater. Electron. 35, 1796 (2024)
- A.M. Jassem, Q.M.A. Hassan, F.A. Almashal, H.A. Sultan, A.M. Dhumad, C.A. Emshary, L.T.T. Albaaj, Spectroscopic study, theoretical calculations, and optical nonlinear properties of amino acid (glycine)-4-nitro benzaldeyhydederived Schiff base. Opt. Mater. 122, 111750 (2021)
- J.K. Salim, Q.M.A. Hassan, A.M. Jassem, H.A. Sultan, A.M. Dhumad, C.A. Emshary, An efficient ultrasoundassisted CH₃COONa catalyzed synthesis of thiazolidinone molecule: theoretical and nonlinear optical evaluations of thiazolidinone-Schiff base derivative. Opt. Mater. 133, 112917 (2022)
- H.A. Abdullmajed, H.A. Sultan, R.H. Al-Asadi, Q.M.A. Hassan, A.A. Ali, C.A. Emshary, Synthesis, DFT calculations and optical nonlinear properties of two derived Schiff base compounds from ethyl-4-amino benzoate. Phys. Scr. 97, 025809 (2022)
- H.H. Al-Hujaj, Q.M.A. Hassan, F.A. Almashal, H.A. Sultan, A.M. Dhumad, A.M. Jassem, C.A. Emshary, Benzenesulfonamide-thiazole system bearing an azide group: Synthesis and evaluation of its optical nonlinear responses. Optik 265, 169477 (2022)
- T.N. Basappa, K.N. Ashoka, K.V. Sathish, S. Brungesh, D. Shashidhar, D.R. Karthik, H. Patwari, A.H. Syed, M.I. Almuqrin, K.N.N. Sayyed, A.G. Prasad, K. Pramod, G. Keshavamurthy, Jagannath, Enhanced nonlinear optical ad optical limiting properties holmium containing borate glasses embedded with silver nanoparticles. J. Mater. Sci. Mater. Electron. 35, 519 (2024)
- U.J. Al-Hamdani, Q.M.A. Hassan, A.M. Zaidan, H.A. Sultan, K.A. Hussain, C.A. Emshary, Z.T.Y. Alabdullah, Optical nonlinear properties and all optical switching in a synthesized liquid crystal. J. Mol. Liq. 361, 119676 (2022)
- S. Kumari, A study of optical modulation and higher transmission capacity. Int. J. Adv. Acad. Stud. 2, 127–129 (2020)
- S. Stopinski, M. Malinosky, R. Piramidowicz, E. Klein, M.K. Smit, X.J.M. Leijten, Integrated optical delay lines for time-division multiplexers. IEEE Photonics J. 5, 7902109 (2013)
- S.K. Khalaf, Q.M.A. Hassan, C.A. Emshary, H.A. Sultan, Concentration effect on optical properties and optical limiting of PVA doped with nigrosin films. J. Photochem. Photobiol. A Chem. 427, 113809 (2022)



- M. Sheik-Bahae, A.A. Said, E.W. Van Stryland, High sensitivity single beam n₂ measurements. Opt. Lett. 14, 955–957 (1989)
- M. Sheik-Bahae, A.A. Said, T. Wei, D.J. Hagan, E.W. Van Stryland, Sensitive measurement of optical nonlinearities using a single beam. IEEE J. Quant. Electron. 26, 760–769 (1990)
- J.P. Gordon, R.C. Leite, R.S. Moore, S.P.S. Porto, J.R. Whinner, Long-transient effect: in lasers with inserted liquid samples. J. Appl. Phys. 36, 3–8 (1965)
- W.R. Callen, B.G. Huth, R.H. Pantell, Optical patterns of thermally self-defocused light. Appl. Phys. Lett. 11, 103– 105 (1967)
- M. Abdul-Bary, B. Haddad, Synthesis and characterization of some new Schiff base containing 4,5-dihydroisoxazole moieties. AIP Conf. Proc. 2213, 020091-1-020091-5 (2020)
- Y. Vibhute, M. Basser, Synthesis and antimicrobial activity of some new chalcones and flavones containing substituted naphthalene moiety. Ind. J. Chem. 42, 202–205 (2003)
- G. Rajendran, D. Bhanu, B. Aruchamy, P. Ramani, N. Pandurangan, K. Bobba, E. Oh, H. Chung, P. Gangadaran, B.C. Ahn, Chalcone: a promising bioactive scaffold in medicinal chemistry. Pharmaceuticals 15, 1250 (2022)
- 32. H. Schiff, Information from the University Laboratory in Pisa: a new range of organic bases. Justus Liebigs Ann. Chem. **131**, 118–119 (1864)
- R. Kalirajan, M. Palanivelu, V. Rajamanickam, G. Vinothapooshan, Synthesis and antimicrobial activities of various pyrazolines from chalcones. Int. J. Chem. Technol. Res. 4, 971–975 (2012)
- S. Aytac, O. Gundogdu, Z. Bingol, I. Gulcin, Synthesis of Schiff bases containing phenol rings and investigation of their antioxidant capacity, anticholinesterase, butyrylcholinesterase, and carbonic anhydrase inhibition properties. Pharmaceuticals 15, 779 (2023)
- A. Al-Azzawi, S. Aziz, E. Dannoun, A. Iraqi, M. Nofal, A. Murad, A.M. Hussein, A mini review on the development of conjugated polymers: steps towards the commercialization of organic solar cells. Polymers 15, 164 (2023)
- M.S. Salem, M. Farhat, A.O. Errayes, M.H. Madkour, Antioxidant activity of novel fused heterocyclic compounds derived from tetrahydropyrimidine derivative. Chem. Pharm. Bull. 63, 866–872 (2015)
- S. Razzaq, A.M. Minhas, N.G. Qazi, H. Nadeem, A. Khan, F. Ali, S.S. Hassan, S. Bungau, Novel isoxazole derivative attenuates ethanol-induced gastric mucosal injury through inhibition of H+/K+-ATPase pump, oxidative stress and inflammatory pathways. Molecules 27, 5065 (2022)

- 38. M. Ordonez, R. Cabrera, C. Cativiela, An overview of stereoselective synthesis of α-aminophosphonic acids and derivatives. Tetrahedron **65**, 1749–1756 (2009)
- S. Arfin, N.K. Jha, S.K. Jha, K.K. Kesari, J. Ruokolainen,
 S. Roychoudhury, D. Kumar, Oxidative stress in cancer cell metabolism. Antioxidants 10, 642 (2021)
- J. Blahova, M. Martiniakov, M. Babikova, V. Kovacova, V. Mondockova, R. Omelka, Pharmaceutical drugs and natural therapeutic products for the treatment of type 2 diabetes mellitus. Pharmaceuticals 14, 806 (2021)
- 41. S. Nilufer, R. Sevim, Synthesis and antituberculosis activity of 2-(aryl/alkylamino)-5-(4-aminophenyl)-1,3,4-thiadiazoles and their Schiff bases. ARKIVOC **12**, 173–181 (2006)
- P. Shamly, P. Mary, A. Anitta, T. Jaya, Synthesis of salicylaldehyde-based Schiff bases and their metal complexes in aqueous media-characterization and antibacterial study. Int. J. Rec. Sci. Res. 9, 26566–26570 (2018)
- 43. G. Dou, P. Xu, Q. Li, Y. Xi, Z. Huang, D. Shi, Clean and efficient synthesis of isoxazole derivatives in aqueous media. Molecules **18**, 13645–13653 (2013)
- 44. A. D. Adesina. Synthesis of Schiff bases by non-conventional methods, in *Schiff Base in Organic, Inorganic and Physical Chemistry* (IntechOpen, 2023)
- S. Bhagat, N. Sharma, T. Chundawat, Synthesis of some salicylaldehyde-based Schiff bases in aqueous media. J. Chem. 2013, 909217 (2013)
- T. Sreevidya, B. Narayana, H. Yathirajan, Synthesis and characterization of some chalcones and their cyclohexenone derivatives. Cent. Eur. J. Chem. 8, 174–181 (2010)
- N. Elkanzi, H. Hrichi, R. Alolayan, W. Derafa, F. Zahou, R. Bakr, Synthesis of chalcones derivatives and their biological activities: a review. ACS Omega 7, 27769–27786 (2022)
- 48. H. Marvaniya, P. Parikh, D. Sen, Synthesis and in-vitro screening of 3,4-dihydropyrimidin-2 (1*H*)-one derivatives for antihypertensive and calcium channel blocking activity. J. Appl. Pharm. Sci. **1**, 109–113 (2011)
- S. Sibous, S. Boukhris, R. Ghailane, N. Habbadi, A. Hassikou, A. Souizi, Easy synthesis of 3,4-dihydropyrimidin-2-(1H)-one derivative using phosphate fertilizers map, dap, and tsp as efficient catalysts. J. Turk. Chem. Soc. 4, 477–488 (2017)
- A. Abu El-Fadl, G.A. Mohamad, A.B. Abd El-Moiz, M. Rashad, Optical constants of Zn_{1-x}Li_xO films prepared by chemical bath decomposition technique. Physica B 366, 44–54 (2005)
- 51. E. Santamato, Y.R. Shen, Field curvature effect on the diffraction ring pattern of laser beam dressed by spatial



2231 Page 22 of 22 J Mater Sci: Mater Electron (2024) 35:2231

- self-phase modulation in animatic film. Opt. Lett. **9**, 564–566 (1984)
- S. Chavez-Cerda, C.M. Nascimento, M.A.R.C. Alencar, M.G.A. da Silva, M.R. Mene Ghetto, J.M. Hickman, Experimental observation of the Far field diffraction pattern of divergent and convergent Gaussian beam in a self-defocusing medium. Ann Opt XXIX, 1–4 (2006)
- L. Deng, K. He, T. Zhou, C. Li, Formation and evolution by far-filed diffraction patterns of divergent and convergant Gaussian beam passing through self-focusing and selfdefocusing media. J. Opt. A Pure Appl. 7, 409–415 (2005)
- Y. Jia, Y. Shan, L. Wu, X. Dai, D. Fan, Y. Xiang, Broadband nonlinear optical resonance and all-optical switching of liquid phase exfoliated tungsten diselenide. Photonics Res. 5, 1040–1047 (2018)
- 55. Q. Wang, X. Wu, L. Wu, Y. Xiang, Broadband nonlinear optical response in Bi₂Se₂-Bi₂Te₃ heterostructure and its application in all-optical switching. AIP Adv. **9**, 025022 (2019)
- X.J. Zhang, Z.H. Yuan, R.X. Yang, Y. He, Y.L. Qin, X. Si, H. Jun, A review on spatial self-phase modulation of twodimensional material. J. Cent. South Univ. 26, 2295–2306 (2019)
- F.L.S. Cuppo, A.M.F. Neto, S.L. Góomez, P. Palffy-Muhoray, Thermal-lens model compared with the

- Sheik-Bahae formalism in interpreting Z-scan experiments on lyotropic liquid crystals. J. Opt. Soc. Am. B **19**, 1342–1348 (2002)
- K. Sendhil, C. Vijayan, M.P. Kothiyal, Low-threshold optical power limiting of cw laser illumination based on nonlinear refraction in zinc tetraphenyl porphyrin. Opt. Laser Technol. 38, 512–515 (2006)
- K. Ogusu, Y. Kohtani, H. Shao, Laser-induced diffraction rings from an absorbing solution. Opt. Rev. 3, 232–234 (1993)
- R. Karimzadeh, Spatial self-phase modulation of a laser beam propagation through liquids with self-induced natural convection flow. J. Opt. 14, 095701 (2012)

Publisher's Note Springer Nature remains neutral with regard to jurisdictional claims in published maps and institutional affiliations.

Springer Nature or its licensor (e.g. a society or other partner) holds exclusive rights to this article under a publishing agreement with the author(s) or other rightsholder(s); author self-archiving of the accepted manuscript version of this article is solely governed by the terms of such publishing agreement and applicable law.

